Quantification of Gypsum Crystal Nucleation, Growth, and Breakage Rates in a Wet Flue Gas Desulfurization Pilot Plant

Brian B. Hansen, Søren Kiil, and Jan E. Johnsson
Dept. of Chemical and Biochemical Engineering, Technical University of Denmark, Lyngby, Denmark

DOI 10.1002/aic.11909
Published online July 24, 2009 in Wiley InterScience (www.interscience.wiley.com).

The aim of this work is to study the influence of nucleation, growth and breakage on the particle size distribution (PSD) of gypsum crystals produced by the wet flue gas desulfurization (FGD) process. The steady state PSD, obtained in a falling film wet FGD pilot plant during desulfurization of a 1000 ppm(v) SO_2 gas stream, displayed a strong nonlinear behaviour (in a ln(n(l)) vs. l plot) at the lower end of the particle size range, compared to the well-known linear mixed suspension mixed product removal model. A transient population balance breakage model, fitted to experimental data, was able to model an increase in the fraction of small particles, but not to the extent observed experimentally. A three-parameter, size-dependent growth model, previously used for sodium sulphate decahydrate and potash alum, was able to describe the experimental data, indicating either size-dependent integration kinetics or growth rate dispersion. © 2009 American Institute of Chemical Engineers *AIChE J*, 55: 2746–2753, 2009
Keywords: FGD, gypsum, particle size distribution, particle breakage, MSMPR

Introduction

The combustion of fossil fuels, such as coal and oil, supply a substantial part of the world's present energy demand and is expected to continue to do so in the coming years.[1] The sulfur present in these fuels is oxidized during combustion thereby forming sulfur dioxide (SO_2), and to a lesser extent sulfur trioxide (SO_3). Oxidation of SO_2 and reaction with water vapour can take place in the atmosphere forming sulfuric acid aerosols. The resulting acid rain has been associated with detrimental effects such as a reduction in atmospheric visibility, damage to buildings, flora and fauna and an increase in the occurrence of respiratory diseases.[2] To reduce these detrimental effects national legislation and international protocols concerning SO_2 emissions have been introduced since the 1970s.[3] These initiatives have triggered the development and installation of a range of flue gas desulfurization (FGD) technologies at power plants all over the world. The majority of the installed FGD capacity consists of the wet scrubber FGD technology,[3] in which the flue gas is brought into contact with a calcium hydroxide solution ($Ca(OH)_2$) or a slurry of calcium carbonate ($CaCO_3$). Additional air is often supplied to the slurry, called forced oxidation mode, ensuring an almost complete conversion of the reactant and the absorbed SO_2 to $CaSO_4 \cdot 2H_2O$ (gypsum). Equation 1 provides the overall reaction of the forced oxidation process.

$$CaCO_3(s) + SO_2(g) + 2H_2O(l) + \frac{1}{2}O_2(g) \rightarrow CaSO_4 \cdot 2H_2O(s) + CO_2(g) \quad (1)$$

Most European power plants use this gypsum producing process because of the gypsum sales potential for either wallboard or cement production. The sales potential will be influenced by material properties such as the particle size distribution (PSD), the impurity content, and the moisture content. These properties will in turn be determined by the crystallization process,[4] which may include: Nucleation, crystal growth (diffusion to and integration of ions into the crystal lattice), crystal agglomeration, crystal breakage and

Correspondence concerning this article should be addressed to S. Kiil at sk@kt.dtu.dk

Table 1. Experimental Conditions

Experiment	Crystal Concentration	Last Sampling
Experiment 1	144.2 g L^{-1}_{slurry} (13.3 wt %)	1.21×10^6 s (336 h)
Experiment 2	75.0 g L^{-1}_{slurry} (7.2 wt %)	2.16×10^6 s (600 h)

size-dependent dissolution (Ostwald ripening). The gypsum produced is withdrawn, washed and dewatered by e.g. hydro cyclones, centrifuges or belt filters, until a commercial product is obtained. Poor dewatering properties may be the result of an increased fraction of small particles (nucleation/breakage) or a change of morphology. Breakage of crystals may take place due to collisions with the reactor walls, the impellor or other particles and fragments ranging in size from nuclei to the size of the parent particle may be formed. Within industrial crystallisers breakage are considered the primary source of nucleation.[5] Previous bench-scale investigations of gypsum crystallization kinetics, at wet FGD conditions, have used McCabe analysis to extract apparent growth and nucleation rates, which have subsequently been fitted to empirical kinetic expressions.[6] This article will expand the present knowledge concerning gypsum crystallization in wet FGD plants, by quantifying the rates of nucleation, crystal growth and crystal breakage taking place in a wet FGD pilot plant and by studying the influence of these processes on the obtained PSD.

Strategy of Investigation

This investigation of the nucleation, crystal growth and breakage in the wet FGD process was performed in a pilot-scale plant. The pilot-scale plant enables a high degree of control of the experimental conditions such as crystal residence time and crystal concentration. The crystal concentrations encountered in industrial plants are usually in the range 10–25 wt %, balancing concerns about bursts of nucleation/scaling and sedimentation/breakage. Depending on the choice of crystal concentration, plant design, and the sulfur content of the fuel the crystal residence time may vary from 7.2×10^4 s (20 h) to more than 3.6×10^5 s (100 h). The 144.2 g L^{-1}_{slurry} (13.3 wt %) gypsum slurry obtained by desulfurization of a 1000 ppm(v) SO_2 gas stream was used to evaluate the crystallization process at a mean slurry residence time ($\bar{t}$) of 1.01×10^5 s (28.13 h). This slurry was furthermore used as starting material in two breakage experiments performed at conditions of industrial relevance (Table 1) and in the absence of FGD, eliminating the effect of crystal growth. Due to sedimentation no experiments above 144 g/L were completed. A three-parameter population balance breakage model was used to describe the experimentally observed changes in PSD as a function of time. The steady state PSD in the pilot plant during desulfurization operation was evaluated based on the breakage model obtained, and estimated values of nucleation rate (B^0) and growth rate (G). Finally, considerations regarding the importance of the different crystallization mechanisms (breakage, size-dependent growth and growth rate dispersion) in the pilot plant as well as conditions at industrial scale were made.

Model Formulation and Solution

The PSD within a crystallizer depends on operating conditions and crystallization processes such as mixing, residence time, nucleation rate, breakage and crystal growth rate. Population balance techniques can be used to simulate the PSD resulting from these conditions.[7] The general population balance for a well-mixed crystallization vessel, in which particle growth, slurry flow and particle birth and death takes place, is given by Eq. 2.

$$\frac{\partial(n(l))}{\partial t} + \frac{\partial(G \cdot n(l))}{\partial l} + \frac{n(l)}{\bar{t}} + n(l) \cdot \frac{d(\ln V)}{dt} = B(l) - D(l) \tag{2}$$

The gypsum crystallization taking place in a wet FGD plant has been evaluated by the following approaches:

- McCabe analysis of steady-sate pilot plant PSD and solid concentration (G and B^0).
- Least squares fitting of breakage kernel parameters based on breakage experiment PSD.
- Evaluation of steady state PSD (Previously estimated G, B^0 and breakage kernel parameters).
- Least squares fitting of size-dependent growth rate parameters based on steady state PSD and solid concentration.

McCabe analysis

The well-known mixed suspension mixed product removal (MSMPR) model, Eq. 3, allows the easy extraction of the growth rate and the nucleation rate from the linear semilogarithmic plot of the population density, $n(l)$, vs. the characteristic particle size, l.

$$n(l) = n(l_0) \cdot \exp\left(\frac{-l}{G \cdot \bar{t}}\right) = \left(\frac{B^0}{G}\right) \cdot \exp\left(\frac{-l}{G \cdot \bar{t}}\right)$$
$$\Rightarrow \ln(n(l)) = \ln\left(\frac{B^0}{G}\right) + \left(\frac{-l}{G \cdot \bar{t}}\right) \tag{3}$$

Several crystallising systems have, however, been reported to display nonlinearity through a considerable curvature, especially at the lower particle sizes.[5,8–11] Such nonlinearity may arise because of shortcomings of any of the assumptions of the MSMPR model: steady state, a constant well-mixed suspension volume, the absence of crystals in the feed stream, no breakage/agglomeration and a size-independent growth rate, i.e. McCabe's Δl law[7]

Breakage modelling

The population balance on a particle volume basis, $n_v(v)$, is used when processes that change the number of particles is of interest (i.e. particle agglomeration or breakage).[7] Equation 4 describes a well-mixed crystallization vessel in which only particle birth and death is taking place.

$$\frac{\partial n_v(v)}{\partial t} = B(v) - D(v)$$
$$= \left(\int_v^{v_{max}} \beta(v,w) \cdot N_b(w) \cdot D(w) \cdot dw\right) - D(v) \tag{4}$$

The birth term consists of the breakage kernel (β), describing the probability of formation of a fragment of

volume "v" from the parent particle volume "w", the number of new particles formed per parent particle [$N_b(w)$] and the death term of the parent particle [$D(w)$]. The breakage kernel may take the form of various mathematical functions[12,13] as well as the very simple two pieces of equal size function used in the literature[4,7] to model breakage processes. In the present study the cumulative Weibull distribution function, Eq. 5, has been used as breakage kernel.

$$F_v(l) = 1 - e^{-(l/\lambda)^{k_{we}}}$$

$$\rightarrow \beta(l_v, l_w) = \frac{\partial F_v(l)/\partial l\Big|_{l_v}}{F_v(l_w)} = \frac{\partial F_v(l)/\partial l\Big|_{l_v}}{0.999} \quad (5)$$

where the parameter k_{we} and λ describes the shape and width of the distribution, respectively. The pieces formed are distributed between the size of the parent particle (l_w), chosen as the 99.9% quantile, and down towards the size of nuclei. A major advantage of the Weibull distribution function is its ability to approximate other distribution functions, such as the exponential distribution function when the shape parameter (k_{we}) is equal to 1. The integral form of the Weibull distribution is the well-known Rosin-Rammler distribution used to describe the cumulative PSD resulting from crushing and milling of materials.[14]

Power law functions are often used in the literature to describe the death term.[4,7] The power law function used in this study, Eq. 6, includes an additional empirical exponent (k_e) to account for the strong particle number and volume dependence observed in the experimental data.

$$D(v) = k_d \cdot v^{k_e} \cdot n_v(v)^{k_e} \quad (6)$$

To facilitate the solution of Eq. 4, the population balance model is discretized into a range of intervals each of which is represented by a characteristic grid point "x". The discretization used in this study is based on the 64 particle size intervals used in the PSD analysis. The lower boundary of the first interval is, however, changed to 0 μm to preserve the mass of the system. The population model is solved by the "SIRUKE" FORTRAN integration routine,[15] based on the initial population density and a given set of kinetic parameters (k_d, k_e, k_{we}, and λ). The width of the Weibull distribution (λ) will not influence the simulation, because the pieces formed will always be distributed between the size of the parent particle (l_w) and down towards the size of nuclei. The remaining kinetic parameters (k_d, k_e, k_{we}) are determined based on a stepwise iteration aiming at a minimization of the sum of least squares of the PSD after 1.21×10^6 s (336 h) of breakage. A 64-interval discretization was sufficient to obtain convergence.

Pilot plant PSD—nucleation, growth, and breakage

The maximal accumulation of fragments at small particle sizes, and thereby the most pronounced impact of breakage, will take place when the fragments only have a limited growth rate. In this work the growth rate of the breakage fragments will therefore be considered negligible compared to the growth rate of crystals formed by nucleation. The formation of slow growing breakage fragments has been proposed previously in the literature[8,9] and has been demonstrated in the case of pentaerythritol[5] and ammonium sulphate[16] crystallization. The assumption of a negligible fragment growth rate furthermore enables a separation of the particle growth and breakage calculations.

The simulation procedure treats one interval at the time and consists of a calculation of the number of crystals entering the interval through growth, Eq. 7, and the particle number being redistributed through breakage, Eqs. 4, 6, and 8. The previously estimated kinetic parameters (G, B^0, k_d, k_e, and k_{we}) alongside a 64-interval discretization have been used for this simulation. The extent of breakage depends on the time the crystals spend in a given interval (t_j). The birth terms require the knowledge of all death terms, and will consequently be calculated as the last part of the simulation. The 64-interval discretization is sufficient to obtain convergence of the solution, as it also was seen for the breakage-only simulation.

$$\rightarrow \ln\left(n(l_j)_{MSMPR}\right) = \ln\left(n(l_{j-1})\right) - \frac{(l_j - l_{j-1})}{G \cdot \bar{t}}$$

$$\text{with } n(l_0) = \frac{B^0}{G} \quad (7)$$

$$n_v(v_j) = n_v(v_j)_{MSMPR} + \left(B(v_j) - D(v_j)\right) \cdot t_j \qquad t_j = \frac{\Delta l_j}{G} \quad (8)$$

Size-dependent growth rate

A semiempirical size-dependent growth rate model, Eq. 9, has been obtained from the literature[17] yielding the steady state MSMPR population density distribution given by Eq. 10.

$$G(l) = G_m(1 - \exp(-a_1(l + a_2))) \quad (9)$$

$$n(l) = n(l_0) \cdot \exp(a_1 \cdot l) \cdot \left(\frac{\exp(a_l(l + a_2)) - 1}{\exp(a_1 \cdot a_2) - 1}\right)^{\frac{-1 - a_1 \cdot \bar{t} \cdot G_m}{a_1 \cdot \bar{t} \cdot G_m}} \quad (10)$$

This three-parameter, size-dependent growth model has previously been used to describe sodium sulphate decahydrate and potash alum crystallization.[17] The empirical model parameters affect the size dependence of the growth rate (a_1) and the growth rate at small crystal sizes (a_2). Input to the simulation procedure is the mean residence time ($\bar{t}$), the population density of nuclei [$n(l_0)$], the maximum growth rate (G_m) and estimates of a_1 and a_2. The empirical parameters of the kinetic model (a_1 and a_2) have been estimated by a stepwise sum of least squares fitting of the PSD and the crystal concentration respectively. The 64-interval discretization is sufficient to obtain convergence of the solution, as it also was seen for the breakage-only and the pilot plant PSD simulations.

Experimental Setup and Procedure

Description of setup

The wet FGD pilot plant simulates a single vertical channel of the packing zone in a co-current full-scale wet FGD grid absorber. The basic outline of the pilot plant is

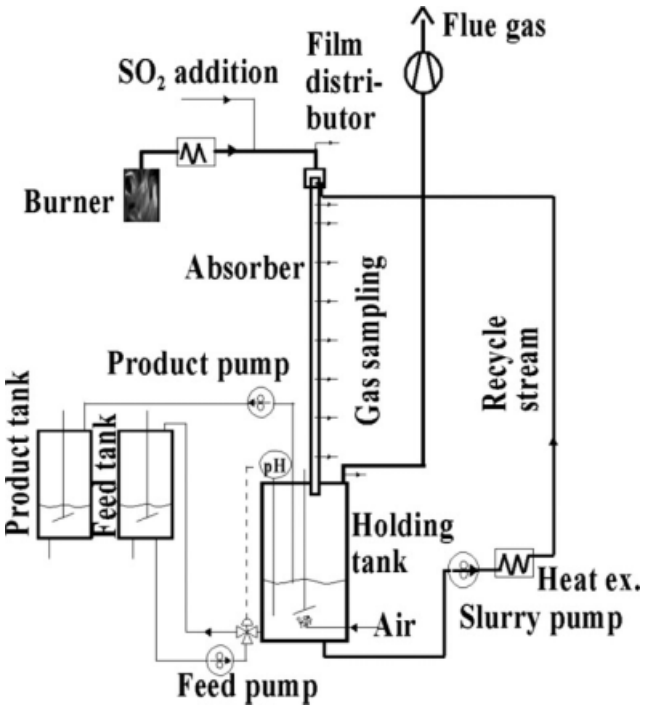

Figure 1. Principal diagram of wet FGD pilot plant.

illustrated in Figure 1. A 110 kW natural gas boiler generates a feed flue gas to which pure SO_2 is subsequently added. The flue gas is brought into contact with limestone slurry in the absorber, a 7 m PVC pipe ($D_i = 3.3$ cm) with multiple sampling sites. The slurry leaving the absorber is collected in a holding tank, $D_i = 0.4$ m, where air injection and reactant addition take place. The pH of the holding tank is kept constant at 5.4 by an on/off control of the feed stream. A timer-controlled pump removes the slurry that exceeds a given level, ensuring a constant slurry level in the tank. From the holding tank the slurry is recycled to the absorber ensuring a liquid/gas ratio of 13.5–14.0 L m^{-3} (STP). Due to the intensive stirring of the holding tank, and because the residence time in the falling film absorber constitutes less than 10% of the residence time in the holding tank, the pilot plant is considered well-mixed. Further details concerning the pilot plant can be seen in a previous publication,[18] but it should be noted that the absorber length has been increased from 5 to 7 m, since that publication, to obtain higher desulfurization degrees.

Experimental procedures

The gypsum slurries used in the breakage experiments have been generated by desulfurization of a 1000 ppm(v) flue gas stream using a feed stream containing 7.1 wt % Faxe Bryozo limestone and 2.2 wt % (25 g L^{-1}) Cl^-. Calcium chloride ($CaCl_2 \cdot 2H_2O$) is used to simulate the presence of Ca^{2+} and Cl^- ions in full-scale wet FGD plants. The Cl^- ions originate from HCl (g) absorbed in the slurry.[19] When the steady state gypsum concentration is obtained, the flue gas flow is turned off and the initial PSD measured. The slurry is now subjected to the continued mechanical inputs from stirring, pumping (recirculation) and air injection. The initial PSD as well as the development over time is measured by laser diffraction with a Malvern Mastersizer S long bed. Two individual PSD analyses were performed on each slurry sample, each representing the average of six measurements. The measurements performed yield the cumulative volume fraction of 64 particle size intervals ranging from 0.05 to 878.67 μm. Experiments have been performed at crystal concentrations of 144.2 and 75.0 g L_{slurry}^{-1} at a constant suspension volume, in the absence of input/output streams, for 1.21 106 s (336 h) and 2.16 $\times$ 10^6 s (600 h) respectively. No particle growth is expected to occur, as no further SO_2 addition takes place after the breakage experiments have been initiated. Selected process parameters of the breakage experiments can be seen in Tables 1 and 2. The PSD measurement and the crystal concentration can be used to calculate the population densities, Eqs. 11 and 12.

$$n(l_j) = \frac{M_{\text{T}} \cdot \left(F_{\text{v}}(l_j) - F_{\text{v}}\left(l_{j-1}\right)\right) / \left(\rho_{\text{s}} \cdot \bar{v}_j\right)}{\Delta l_j} \tag{11}$$

$$n_{\text{v}}(v) = n(l) \cdot \frac{dl}{dv} = n(l) \cdot \frac{1}{A_{\text{su}}} \tag{12}$$

An overview of the changes in PSD as a function of time can be obtained by monitoring the development of a suitable mean diameter. Due to the importance of the dewatering properties of the gypsum the Sauter mean diameter (SMD) is chosen as the mean diameter of interest. The SMD describes the diameter of a sphere with the same surface area to volume ratio as the particle investigated and is reported[20] to be the appropriate average particle size in the case of fluid flow through porous media, such as the solid liquid separation in dewatering processes.

Results and Discussion

McCabe analysis

The steady state PSD in the pilot plant is evaluated based on experimental data obtained after 5.15 $\times$ 10^5 s (143 h) of desulfurization of a 1000 ppm(v) SO_2 flue gas stream at a liquid to gas ratio of 13.8 L Nm^{-3}. The mean slurry residence time ($\bar{t}$) was 1.01 $\times$ 10^5 s (28.13 h) corresponding to operation for 5.1 residence times. A simple mass balance of a well-mixed vessel shows that 5.1 residence times corresponds to 99.3% of the steady state crystal concentration. Figure 2 shows the population density obtained by the use of Eq. 11, assuming spherical particles.

A considerable curvature, compared to the MSMPR model, is observed below particle sizes of 25 μm, as it has also been reported for other crystallising systems.[5,8–11] As previously mentioned crystal breakage is one of the potential explanations of this phenomenon. Above a particle size of

Table 2. Selected Process Parameters

Parameter	
Slurry volume	30 L
Recycle stream	0.078 L s^{-1}
Air injection	0.233–0.267 L (STP) s^{-1}
Stirring rate	310 RPM

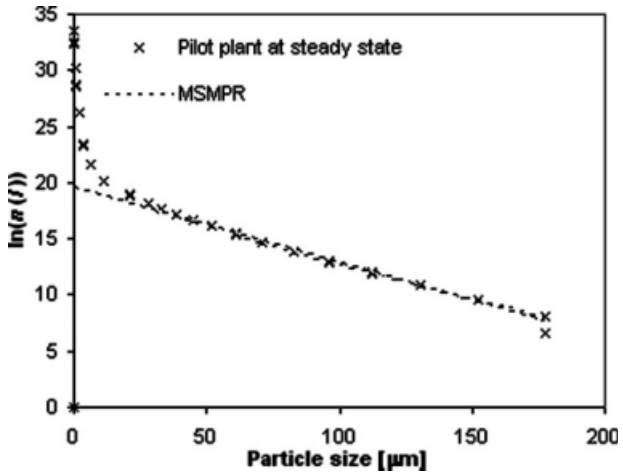

Figure 2. Semi logarithmic plot of population density (Experimental and MSMPR-model) vs. particle size.

Steady state measurements have been performed on the slurry formed by desulfurization of a 1000 ppm(v) gas stream.

25 μm the PSD data points show a linear behavior and a growth rate and a nucleation rate can be extracted by McCabe analysis. The mean growth and nucleation rates are presented below alongside the corresponding analytical standard deviations. Because of the population density deviation at the small particle sizes the mass concentration calculated for the MSMPR system will be lower than the experimental measurements. The nucleation rate in a MSMPR system required to obtain the measured crystal concentration of 144.2 g L^{-1}_{slurry} is shown in parenthesis and will be used in the simulations.

- $G = 1.44 \times 10^{-4} \pm 0.06 \times 10^{-4}$ μm s^{-1}.
- $B^0 = 5.44 \times 10^4 \pm 0.44 \times 10^4$ no. L^{-1}_{slurry} s^{-1} (6.25×10^4 no. L^{-1}_{slurry} s^{-1}).

Breakage modelling

In the breakage experiments performed the changes in PSD of the gypsum slurry has been monitored as a function of the time it has been exposed to the continued mechanical inputs from stirring, pumping (recirculation) and air injection. The changes observed can be used to describe the extent as well as the type of breakage taking place in the pilot plant.

Figure 3 shows the volumetric PSD frequency plotted as a continuous curve with a logarithmic scale on the x-axis at three selected times during experiment 1. The frequency curve describes the change in cumulative volume fraction [$F_v(l)$] as a function of the change in logarithmic particle size. This representation is well suited for showing PSDs covering wide size ranges.[21] The changes in the PSD frequency curves show a decrease in the volume fraction of particles above $\sim$25 μm and a corresponding increase in the volume fraction of particles below this particle size. This corresponds well with the fact that an increased fraction of this size range is observed at steady state. The size of the new particles varies from the submicron range to particles of several microns. The formation of such a wide range of particle sizes indicates that the breakage mechanism is not the simple breakage of a particle into a few large pieces, such as the two-piece breakage mechanism mentioned previously. This breakage behavior is better described by mathematical distribution functions.

The SMD development of both experiments is shown in Figure 4. A decreasing trend as a function of time is observed, corresponding to an increase in the fraction of small crystals and thereby a deterioration of the dewatering potential. The observed trend is pronounced during the initial $\sim 7.2 \times 10^5$ s (200 h) of the experiments and slows down later, most likely as a consequence of the decreased concentration of large particles. The only exception to this decreasing trend is the sudden and unexpected increase in SMD after 8.64×10^4 s (24 h) of mechanical inputs in experiment 2. No particles smaller than 1 μm were present in this sample, indicating that dissolution might have been taking place. The higher particle concentration of experiment 1, and thereby the increased likelihood of particle–particle collisions, causes a steeper initial decrease in the SMD in this experiment.

Based on the previously described solution procedure two sets of kinetic parameters (k_d, k_e, k_{we}) have been determined by a stepwise iteration of the parameters aiming at a minimization of the sum of least squares of the PSD after 1.21×10^6 s (336 h) of the two breakage experiments.

- Experiment 1:
$k_d = 0.094\ L^{0.5}_{slurry} \cdot no^{-0.5} \cdot dm^{-3}\ s^{-1}$
$k_e = 1.55$
$k_{we} = 1.09$
- Experiment 2:
$k_d = 0.442\ L^{0.5}_{slurry} \cdot no^{-0.5} \cdot dm^{-3}\ s^{-1}$
$k_e = 1.49$
$k_{we} = 1.20$

The kinetic parameters obtained show that different combinations of k_d and k_e are able to describe the experimental

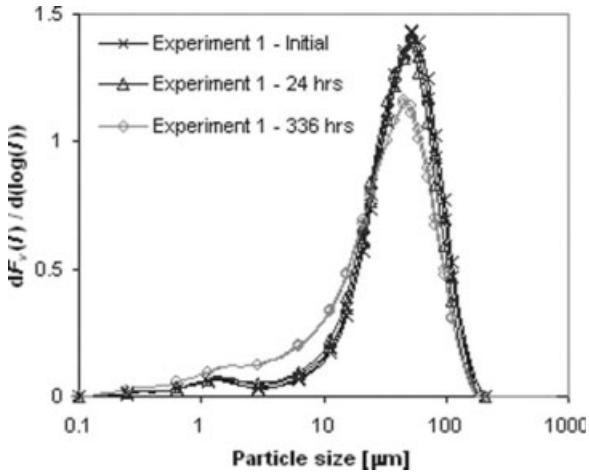

Figure 3. Frequency distribution curves at selected times during breakage experiment 1.

Experimental conditions are provided in Tables 1 and 2. Note that both the points and the continuous curves represent experimental measurements.

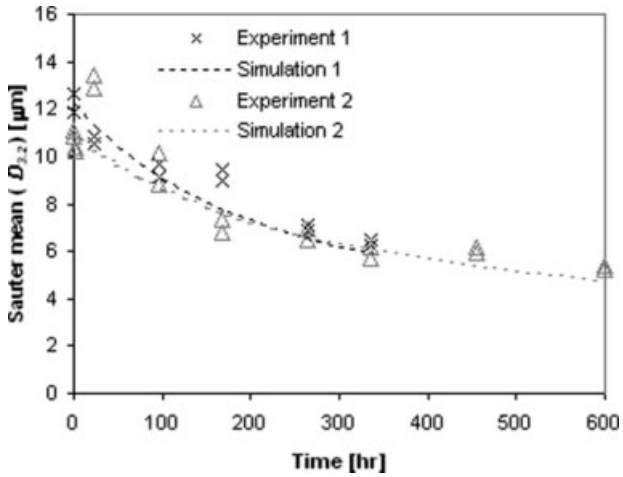

Figure 4. Dynamic development of simulated and experimental SMD in breakage experiment 1 (144.2 g L^{-1}) and 2 (75 g L^{-1}).

Experimental conditions are provided in Tables 1 and 2.

data and that a strong dependence on the particle concentration ($k_e > 1$) exists. No duplicate breakage experiments were performed and so it was not possible to assess parameter uncertainties. However, as it will be shown later, very precise parameter values are not needed because particle breakage is not significant during the slurry residence times used in wet FGD plants. Figure 4 shows the simulated development in SMD as well as the experimental measurements. Simulations are in good qualitative agreement with the experimental data and predict the stronger decrease of SMD in experiment 1 compared to experiment 2 as well as the slower decrease of SMD with time. A slight under-prediction of the SMD of both experiments are observed at long exposure times. Figure 5 illustrates the simulated and the measured PSD frequency curves at selected points in time during breakage experiment 1. The simulated PSD frequency curves are in good agreement with the experimental

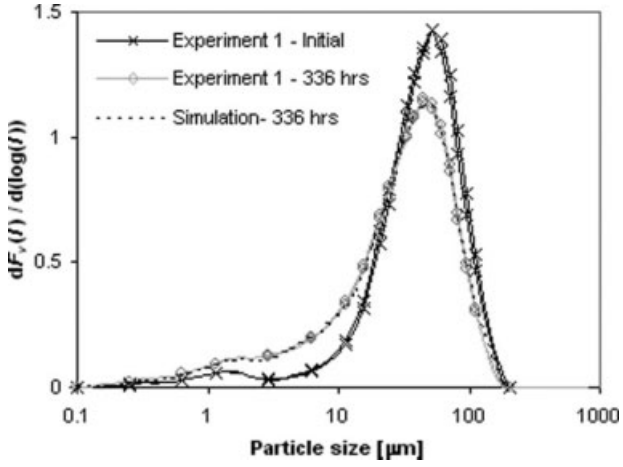

Figure 5. Experimental and simulated frequency distribution curves of breakage experiment 1 [0 s and 1.21 10^6 s (336 h)], experimental conditions are provided in Tables 1 and 2.

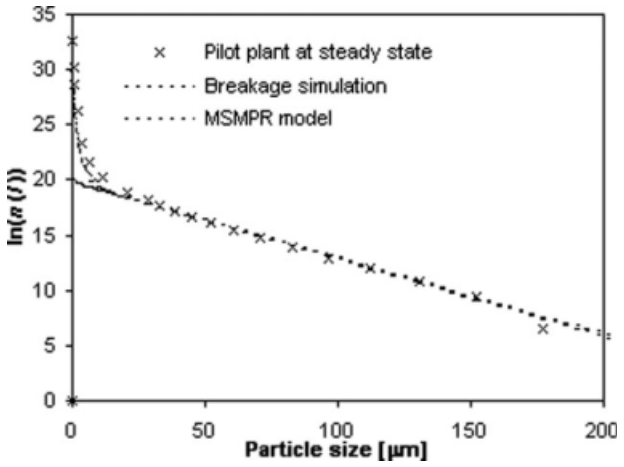

Figure 6. Semi logarithmic plot of the population density vs. particle size (Experimental and growth and breakage simulation).

Steady state measurements has been performed on the slurry formed by desulfurization of a 1000 ppm(v) gas stream. Kinetic parameters: $G = 1.44 \times 10^{-4}$ µm s^{-1}, $\bar{t} = 1.01 \times 10^5$ s (28.13 h), $B^0 = 6.58 \times 10^4$ no. L_{slurry}^{-1} s^{-1}, $k_d = 0.094$ $L_{slurry}^{0.5}$ $no^{-0.5}$ dm^{-3} s^{-1}, $k_e = 1.55$, and $k_{we} = 1.09$.

ones, showing a similar disappearance of particles above ~25 µm and a corresponding increase in particles from about 25 µm down to the submicron range in both experiments.

Pilot plant PSD—nucleation, growth, and breakage

Based on the derived breakage kinetics, the influence of breakage on the steady state PSD of the wet FGD pilot plant has been evaluated. Input to the simulation procedure is the kinetic breakage parameters determined in the transient experiments (k_d, k_e, and k_{we}), the mean residence time [$\bar{t} = 1.01 \times 10^5$ s (28.13 h)] and the crystal growth rate obtained by the McCabe analysis. The nucleation rate has been determined based on a fitting of the particle concentration (144.2 g L_{slurry}^{-1}).

The population density plot obtained, Figure 6, show that an increased number of small particles and thereby a curvature of the semi logarithmic population plot. The PSD plot, Figure 7, does, however, show that simulated volume fraction of fines is significantly lower than the experimental measurements. This indicates that breakage is not the only source of the increased fraction of small particles in the pilot plant PSD compared to the MSMPR model. A finite growth rate of the fragments would only further increase the disagreement between the simulations and the experimental results.

Pilot plant PSD and the influence of size dependent growth

The influence of size-dependent growth on the steady state PSD of the wet FGD pilot plant has furthermore been evaluated. Input to the simulation procedure is the mean residence time ($\bar{t}$), the population density of nuclei [$n(l_0)$] (estimated from the experimental data), the maximum growth rate (G_m) from the McCabe analysis and the empirical model

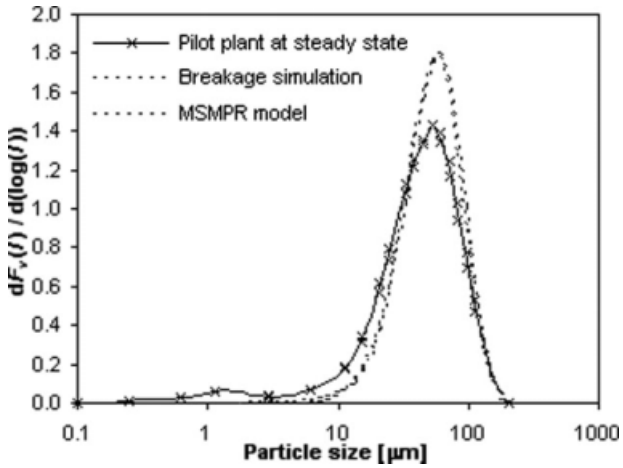

Figure 7. Experimental and simulated (Growth and breakage) frequency distribution curves at steady state desulfurization of a 1000 ppm(v) gas stream.

Kinetic parameters: $G = 1.44 \times 10^{-4}$ μm s^{-1}, $\bar{t} = 1.01 \times 10^5$ s (28.13 h), $B^0 = 6.58 \times 10^4$ no. L_{slurry}^{-1} s^{-1}, $k_d = 0.094$ $L_{slurry}^{0.5}$ no$^{-0.5}$ dm^{-3} s^{-1}, $k_e = 1.55$, and $k_{we} = 1.09$.

parameters (a_1 and a_2) from a stepwise sum of least squares fitting of the PSD and the crystal concentration respectively. The following model parameters were obtained by the sum of least squares fitting procedure (step-size in parenthesis):

- a_1 = 0.057 (0.001) μm^{-1}
- a_2 = 0.039 (0.001) μm

The system shows a strong size-dependence (i.e. a low a_1-value). Figures 8 and 9 show the obtained population density and PSD plots. The simulations and the experimental results agree well down to a particle size of a few microns. Below this particle size the model is, however, unable to describe the increased levels of fines observed. A considerable measurement uncertainty is, however, also expected at these small particle sizes.

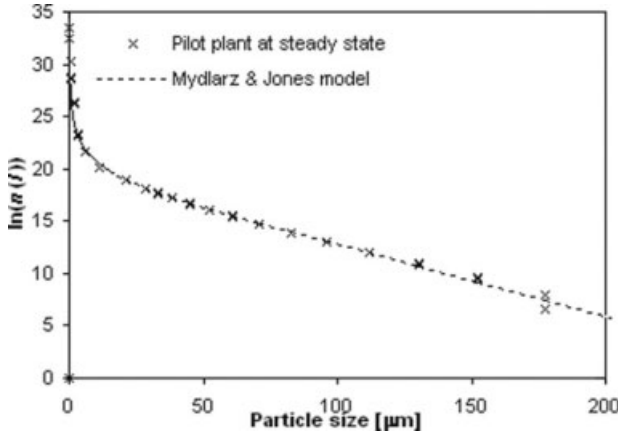

Figure 8. Semi logarithmic plot of the population density vs. particle size (Experimental and size-dependent growth simulation).

Steady state measurements has been performed on the slurry formed by 5.1 residence times desulfurization of a 1000 ppm(v) gas stream. Kinetic parameters: $G_m = 1.44 \times 10^{-4}$ μm s^{-1}, $\bar{t} = 1.01 \times 10^5$ s (28.13 h), $n(l_0) = 2.15 \times 10^{14}$ no. μm^{-1} L_{slurry}^{-1}, $a_1 = 0.057$ μm^{-1}, and $a_2 = 0.039$ μm.

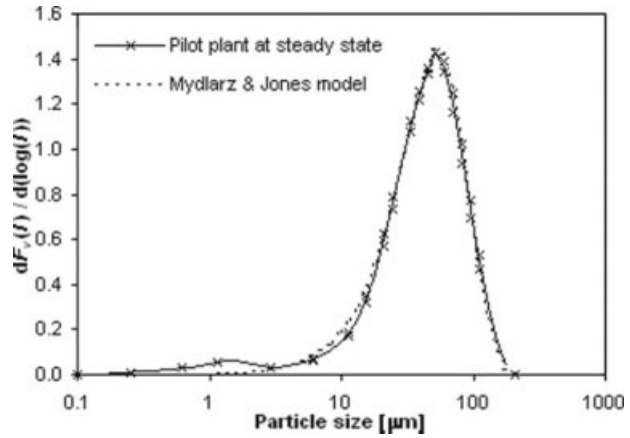

Figure 9. Experimental and simulated (size-dependent growth) frequency distribution curves at steady state desulfurization of a 1000 ppm(v) gas stream.

Kinetic parameters: $G_m = 1.44 \times 10^{-4}$ μm s^{-1}, $\bar{t} = 1.01 \times 10^5$ s (28.13 h), $n(l_0) = 2.15 \times 10^{14}$ no. μm^{-1} L_{slurry}^{-1}, $a_1 = 0.057$ μm^{-1}, and $a_2 = 0.039$ μm.

A size dependent growth rate of particles larger than 100 μm has, in the case of a diffusion controlled reaction, been explained in the literature by the higher particle settling velocity and thereby thinner boundary layers.[22,23] Below a particle size of 50 μm and in well-stirred systems, as in this study, this mechanism is considered unlikely.[11] Crystals smaller than a few microns may have a lower effective growth rate, due to an enhanced dissolution rate, i.e. Gibbs Thomson effect.[16] However in the size range studied, size-dependent surface integration kinetics is considered the most likely explanation. An increasing number of dislocations, and thereby an enhanced surface integration rate, may be present in large crystals due to mechanical stress, impurity incorporation and an increased likelihood of collisions and surface damage.[10,22] However, growth rate dispersion of secondary nuclei, through differences in dislocation concentration (facilitates growth) and integral stress (inhibits growth), may also yield an apparently size-dependent growth rate.[24]

Conclusions

This investigation of the PSD in a wet FGD pilot plant has demonstrated that increased levels of small particles are present compared to the predictions of the simple MSMPR model by Randolph and Larson.[7] Experiments concerning the breakage process have been carried out and a population balance model describing the redistribution of particles derived. Simulations show that the breakage process is unable to generate the increased levels of fine particles observed in the pilot plant. A three-parameter empirical size dependent growth model is able to describe the experimental data down to a particle size of a few microns. Size-dependent integration kinetics or growth rate dispersion of secondary nuclei, due to dislocations and integral stress, is considered the most likely explanations of the apparently size dependent crystal growth rate.

The influence of breakage on the crystallization process taking place at full-scale wet FGD plants will be influenced by the mechanical inputs to the system (stirring and pumping) as well as operating conditions such as the solid concentration, residence time and the presence of growth inhibiting species. The optimal operating conditions in terms of gypsum crystallization will most likely be plant specific and time dependent due to these effects.

Acknowledgments

The authors thank Carsten Nørby for technical assistance. The work presented in this article was performed within the CHEC (Combustion and Harmful Emission Control) Research Center funded a.o. by the Technical University of Denmark, the Danish Technical Research Council, the European Union, the Nordic Energy Research, Dong Energy A/S, Vattenfall A.B., F L Smidth A/S, and Public Service Obligation funds from Energinet.dk and the Danish Energy Research program.

Notation

a_1 = empirical parameter in Mydlarz and Jones growth model (μm^{-1})
a_2 = empirical parameter in Mydlarz and Jones growth model (μm)
A = area (m^2)
B^0 = nucleation rate (no. L_{slurry}^{-1} s^{-1}]
$B(v)$ = birth term (no. dm^{-3} L_{slurry}^{-1} s^{-1})
$B(l)$ = birth term (no. μm^{-1} L_{slurry}^{-1} s^{-1})
D = diameter (m)
$D_{3,2}$ = Sauter mean diameter (μm)
$D(v)$ = death term (no. dm^{-3} L_{slurry}^{-1} s^{-1})
$D(l)$ = death term (no. μm^{-1} L_{slurry}^{-1} s^{-1})
F_v = cumulative volume fraction of particles (−)
G = linear crystal growth rate (μm s^{-1})
G_m = maximal linear crystal growth rate (μm s^{-1})
k_d = breakage rate constant ($L_{slurry}^{0.5}$ $no^{-0.5}$ dm^{-3} s^{-1})
k_e = empirical breakage rate parameter (−)
k_{we} = Shape parameter of Weibull function (−)
l = characteristic particle length (μm)
M_T = slurry density (g $L_{suspension}^{-1}$)
$n(l)$ = population density in length coordinates (no. μm^{-1} L^{-1})
$n(l_0)$ = population density of nuclei in length coordinates (no. μm^{-1} L^{-1})
$n_v(v)$ = population density in volume coordinates (no. dm^{-3} L^{-1})
N_b = number of fragments formed per parent particle (no dm^{-3})
Q = flow rate (L s^{-1})
t = time (s)
$\bar{t}$ = mean residence time e.g. V/Q (s)
V = suspension volume (L)
v = particle volume (dm^3)
$\bar{v}$ = mean volume (dm^3)
w = parent particle volume (m^3)
x = characteristic grid point

Greek letters

β = breakage kernel (−)
Δl_j = size/width of particle size interval "j" (μm)
ρ = density (g dm^{-3})
λ = scale parameter of Weibull distribution (−)

Subscripts

i = inner
j = interval j
max = maximal
MSMPR = mixed suspension mixed product removal model
su = surface
v = corresponding to volume v
w = corresponding to volume w

Literature Cited

1. World energy outlook. Paris: International Energy Agency (IEA) and Organization for Economic Co-operation and Development (OECD), 2004.
2. Wark K, Warner CF, Davis WT. *Air Pollution—Its Origin and Control*, 3rd ed. Addison Wesley Longman, 1998.
3. Soud HN. *Developments in FGD*. London: IEA Coal Research, 2000.
4. Myerson AS. *Handbook of Industrial Crystallization*, 2nd ed. Woburn: Butterworth-Heinemann, 2002.
5. Bujac, PDB. Attrition and secondary nucleation in agitated crystal slurries. In: Mullin, JW. *Industrial Crystallization* (6th symposium on industrial crystallization). New York and London: Plenum Press, 1976:23–31.
6. Randolph AD, Etherton D. Study of gypsum crystal nucleation and growth rates in simulated flue gas desulfurization liquors—EPRI report EPRI-CS-1885. Tucson, AZ: Arizona University–Department of Chemical Engineering, 1981.
7. Randolph AD, Larson MA. *Theory of Particulate Processes—Analysis and Techniques of Continuous Crystallization*, 2nd ed. New York: Academic Press, 1988.
8. Berglund KA, deJong EJ. The calculation of growth and nucleation kinetics from MSMPR crystallizer data including growth rate dispersion. *Sep Technol*. 1990;1:38–45.
9. Kougoulos E, Jones AG, Wood-Kaczmar MW. Estimation of crystallization kinetics for an organic fine chemical using a modified continuous cooling mixed suspension mixed product removal (MSMPR) crystallizer. *J Cryst Growth*. 2005;273:520–528.
10. Garside J, Jancic SJ. Growth and dissolution of potash alum crystals in the subsieve size range. *AIChE J*. 1976;22:887–894.
11. Garside J, Jansen-Van Rosmalen R, Bennema P. Verification of crystal growth rate equations. *J Cryst Growth*. 1975;29:353–366.
12. Bao Y, Zhang J, Yin Q, Wang J. Determination of growth and breakage kinetics of L-threonine crystals. *J Cryst Growth*. 2006;289:317–323.
13. Kostoglou M, Dovas S, Karabelas AJ. On the steady-state size distribution of dispersions in breakage processes. *Chem Eng Sci*. 1997;52:1285–1299.
14. Brown WK, Wohletz KH. Derivation of the Weibull distribution based on physical principles and its connection to the Rosin-Rammler and lognormal distributions. *J Appl Phys*. 1995;78:2758–2763.
15. Villadsen J, Michelsen ML. *Solution of Differential Equation Models by Polynomial Approximation*. New York: Prentice-Hall, 1978.
16. Virone C, ter Horst JH, Kramer HJM, Jansens PJ. Growth rate dispersion of ammonium sulphate attrition fragments. *J Cryst Growth*. 2005;275:1397–1401.
17. Mydlarz J, Jones AG. On the estimation of size-dependent crystal growth rate functions in MSMPR crystallizers. *Chem Eng J*. 1993;53:125–135.
18. Kiil S, Michelsen ML, Dam-Johansen K. Experimental investigation and modelling of a wet flue gas desulfurization pilot plant. *Ind Eng Chem Res*. 1998;37:2792–2806.
19. Kiil S, Nygaard H, Johnsson J. Simulation studies of the influence of HCl absorption on the performance of a wet flue gas desulfurization pilot plant. *Chem Eng Sci*. 2002;57:347–354.
20. Holdich R. *Fundamentals of Particle Technology*. Leicestershire: Midland Information Technology and Publishing, 2002.
21. Allen T. *Particle Size Measurement, Vol. 1*, 5th ed. London: Chapman & Hall, 1997.
22. Mullin JW. *Crystallization*, 4th ed. Oxford: Elsevier Butterworth-Heinemann, 2004.
23. Ulrich J. Solution crystallization—developments and new trends. *Chem Eng Technol*. 2003;26:832–835.
24. Sherwood JN, Ristic RI. The influence of mechanical stress on the growth and dissolution of crystals. *Chem Eng Sci*. 2001;56:2267–2280.

Manuscript received Apr. 8, 2008, and revision received Mar. 10, 2009.